

Improve the energy efficiency of PV systems by installing a soft switching boost converter with MPPT control

Basim Talib Kadhem, Sumer Sahib Harden, Osama Yaseen Khudair Al-Atbee,
Khalid Mahdi Abdulhassan

Department of Electrical Engineering, University of Basrah, Basrah, Iraq

Article Info

Article history:

Received Oct 9, 2022

Revised Dec 13, 2022

Accepted Dec 25, 2022

Keywords:

DC-DC boost converter soft
switching
MPPT
P&O
Photovoltaic
PWM converter

ABSTRACT

To improve the energy consumption rate of solar cells and reduce switching loss, a maximum power point tracking (MPPT) control approach is presented to manage the boost converter and achieve soft switching. A method for determining the optimal values of the soft switching boost converter design parameters has been proposed, by determining the ideal values for the inductor, capacitor, and duty cycle of the boost converter with soft switching, this method enables the key matching of the PV system with the DC/DC converter configuration. In addition to presenting an analysis of several MPPT methodologies, the entire design of the PV converter system is also included. This study compares the perturb-and-observe (P&O) method and the incremental conductance (IC) method for maximum power point tracking (MPPT) in the MATLAB/Simulink application. The PV systems with both MPPT algorithms have been simulated beginning with an implemented model of the photovoltaic (PV) array together with the soft switching boost converter and its MPPT control. The simulation results based on irradiance and temperature are then shown. In the end, soft-switching is more efficient than hard-switching, especially when operating at full load.

This is an open access article under the [CC BY-SA](https://creativecommons.org/licenses/by-sa/4.0/) license.



Corresponding Author:

Sumer Sahib Harden

Department of Electrical Engineering, University of Basrah

PO Box 49, Basrah, Al Basrah, Iraq

Email: sumer.hardan@uobasrah.edu.iq

1. INTRODUCTION

Research and development of alternative energy sources that are cleaner, renewable, and have less impact on the environment have been sparked by the rising demand for energy and the potential for limited availability of conventional fuels [1]. Due to the ongoing price decline of PV modules and the rise in solar PV cell efficiency, solar photovoltaic (PV) power systems have become the most extensively used electricity sources worldwide [2]. Photovoltaic (PV) technology, which has grown in popularity, has been adopted by many industrial purposes, from small battery chargers to massive power plants supplying electricity for the electric power grid. A viable alternative for feeding future smart grids and smart cities is PV applications, which are regarded as a sustainable energy source [3]–[6]. Making PV systems competitive with traditional power sources that produce electricity using fossil fuels has become a recent problem [7]–[9]. This objective could be accomplished by lowering the cost of the PV system's components (PV modules and soft switching boost converters) as well as increasing conversion efficiency. Because it is the most significant component affecting the total efficiency of PV systems, the soft switching DC-DC boost converter efficiency has caught the attention of researchers and engineers [10]–[13]. The negative impacts associated with the second disadvantage may be significantly reduced if the magnitude of the duty-cycle perturbations are matched to the

dynamic behavior of each DC-DC converter used to generate the P&O MPPT [14], [15]. Gaining the greatest power from solar panels for a range of loads may be accomplished by comparing the boost DC-DC converter's performance to that of other converters. The three main kinds of loads that are taken into consideration are constant resistive loads, constant voltage loads, and constant current loads [16]–[18]. To improve the overall optimality of the solar power data as well as the system on which it is used, the (P&O) algorithm, a highly effective MPPT technique, was carried out using a solar PV array coupled to a boost converter. A brief comparison of the approach used with other well-known MPPT processes is also included in the mechanism [19].

Figure 1 shows the widely used zero voltage switching (ZVS) and zero current switching (ZCS) converter with maximum power tracking MPPT. The losses of the semiconductor switching devices employed in the converter are linked to the losses of the DC/DC converter. The losses in the boost converter are represented by the switching losses and the conduction losses. Conduction losses are related to the drop voltage across each switch while turning on, while switching losses are proportional to switching frequency. The power, voltage, and current ratings of the DC-DC converter are included in the converter specifications. The converter efficiency curve, which depicts the relationship between output power and converter efficiency, is also included. The efficiency is highest when the output power of the converter is close to its rated power, and it is lowest when the converter output is low. The PV array rated power which is typically provided during standard test settings, is proportional to the converter input power (STC). The PV cell temperature (TC), which is 25 °C, and the reference solar radiation (G), which is 1000 W/m² [5], [20], [21], are the two main components of the STC. When conditions are realistic, TC is greater than 25 °C and G is less than 1000 W/m². As a result, the PV output power drops when the TC exceeds 25 °C and the G drops below 1000 W/m². The converter will function at lower conversion efficiency in the event where the PV array rated power and output power rated of the converter are set to be equal. As a result, the PV array was specifically created to have a rated power greater than the output power rated of the converter, as depicted in Figure 1. This study presents a method for controlling the switching period and switching loss. Perturbation and observation (P&O) and linear incremental conductance (IC) algorithm with ZVS and ZCS boost converter, a tracked control mechanism with increased steady-state accuracy and environmental adaptability, are one of the important strategies in this system. The two techniques are thoroughly discussed in this work, together with simulation results generated MATLAB and Simulink.

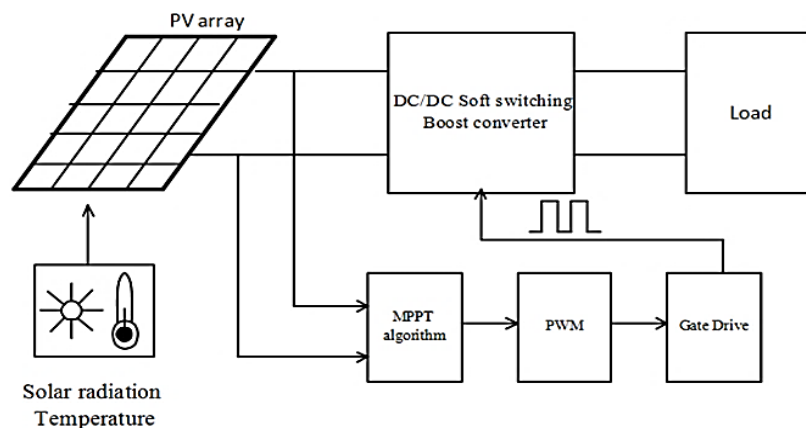


Figure 1. PV grid connected system components and control

2. DESCRIPTION OF THE PROPOSED SYSTEM AND MATHEMATICAL MODELLING

Maximum power point tracking (MPPT) and a DC/DC power converter with soft switching make up the power converter's features in a PV system. A PV generation setup is present in the system, which can take the form of a single module, a string of modules connected in series, or a collection of strings connected in parallel. Today, there is a considerable demand for PV converters, which are produced in a variety of topologies including efficiency improvement of connected PV with the soft switching boost converter. For PV plants (10 to 250 kW and more), the arrangement of series/parallel connections of PV modules with DC/DC power converter is typical and provides great efficiency. When sunlight strikes solar cells, current flows across them. For any given ambient temperature, sunlight intensity, and other internal characteristics, a solar cell is modelled in this article. A similar circuit is created to make it simple to analyze solar cells. When exposed to sunlight, the PV cell, an electrical device that is coupled to a boost converter, generates electrical power. In the suggested model, the current is seen as a controlled source of constant current, and the voltage varies according to the

intensity of the radiation. As a result, Figure 2 depicts the same model PV array using an MPPT controller and a boost converter with soft switching. The boost converter plays a crucial function in modulating the terminal voltage of the PV array in response to changes in duty cycle. As it is mentioned in the next sections, the duty cycle will be decided based on the signal of the maximum power point tracker, whether it is P&O or IC algorithm. When the input voltage is too high and needs to be decreased to a suitable level, buck converters are frequently utilized. In many technical applications, a step down converter is needed to transform a fixed-voltage DC source into a variable-voltage DC output. A step-down converter results in a lower average output voltage than the DC input voltage. Simply referred to as a DC converter, Using a DC-DC switching converter, voltage is directly changed from DC to DC. A DC converter is the same as an AC transformer with a constantly adjustable turn ratio. As a transformer, it can be used to step up or step down a DC voltage source. For the purpose of controlling the traction motor, DC converters are frequently employed in electric cars, trolleys, marine hoists, forklift trucks, and mine haulers. They provide excellent acceleration control, high efficiency and quick dynamic response. They can be applied to DC motors to provide regenerative braking, which returns energy to the power source. This multiple-step characteristic helps transportation systems conserve energy. In addition to being utilized in DC voltage regulators, DC converters can also be used to provide a DC current source, specifically for the current source inverter, by working in tandem with an inductor [8].

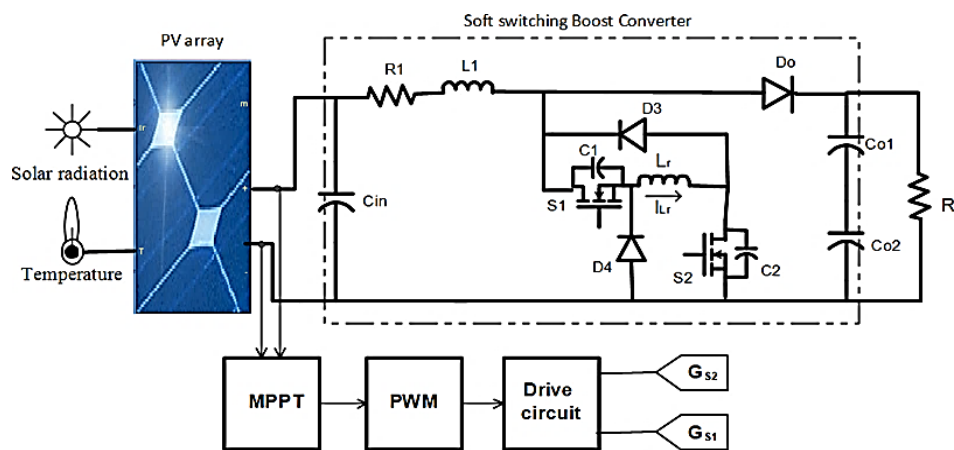


Figure 2. PV array by MPPT controller and boost converter with soft switching

2.1. PV array

The efficiency of energy conversion is still insufficient, and the initial cost of implementation is still considered to be significant, despite all the advantages connected with the use of PVs for energy generation. In order to obtain the highest operating efficiency, it is vital to employ techniques that extract the most electricity from these panels. It is important to note that the MPP, also known as the point of maximum power, is just one and changes in the weather. When load changes are taken into account, it is hard to get the most power out of photovoltaic because the power characteristics are not linear, as shown in Figure 3. These characteristics change with temperature and solar irradiation levels. A comprehensive comparison of the various ways of extracting the maximum power has been suggested in the literature [22]–[25] as a solution to this issue, and the results can provide valuable information for the design of these systems. This paper uses forms created in MATLAB/Simulink in order to evaluate the primary MPPT strategies described in the literature. It then compares the techniques in-depth based on the number of sensors needed, the voltage changes in steady state, the startup of the method, and how much energy is taken out. Obtaining the highest power is a challenging task when load changes are taken into account since the characteristics of photovoltaic power are not linear, as illustrated in Figure 3. These characteristics change with temperature and solar irradiation levels. Numerous strategies for obtaining the maximum power have been put out in the literature [21].

2.2. Main MPPT control methods

In this part, the techniques of fixed duty cycle, constant voltage, perturb and observe (P&O), incremental conductance (IC), ripple correlation, and system oscillation are briefly described. Because the load impedance only needs to be modified once to locate the maximum power point and then it doesn't need to be changed again, the fixed duty cycle technique is the simplest because it doesn't require any feedback. According to empirical data from the constant voltage approach, under typical atmospheric circumstances, the voltage at

MPP (VMPP) is between 70% and 80% of the PV open circuit voltage (VOC). The voltage at the module's terminals fluctuates relatively little among the MPP sites (different atmospheric conditions), even while the amount of solar energy varies. On the other hand, the VMPP rigorously adjusts in response to temperature variations. As a result, alternate data must be accepted and assessed for a variety of geographic and environmental circumstances because the operational point is never precisely at the MPP. The fact that just one voltage sensor is required and that it offers excellent performance with little insulation is an interesting feature. This strategy may be coupled with others to boost efficiency for this reason.

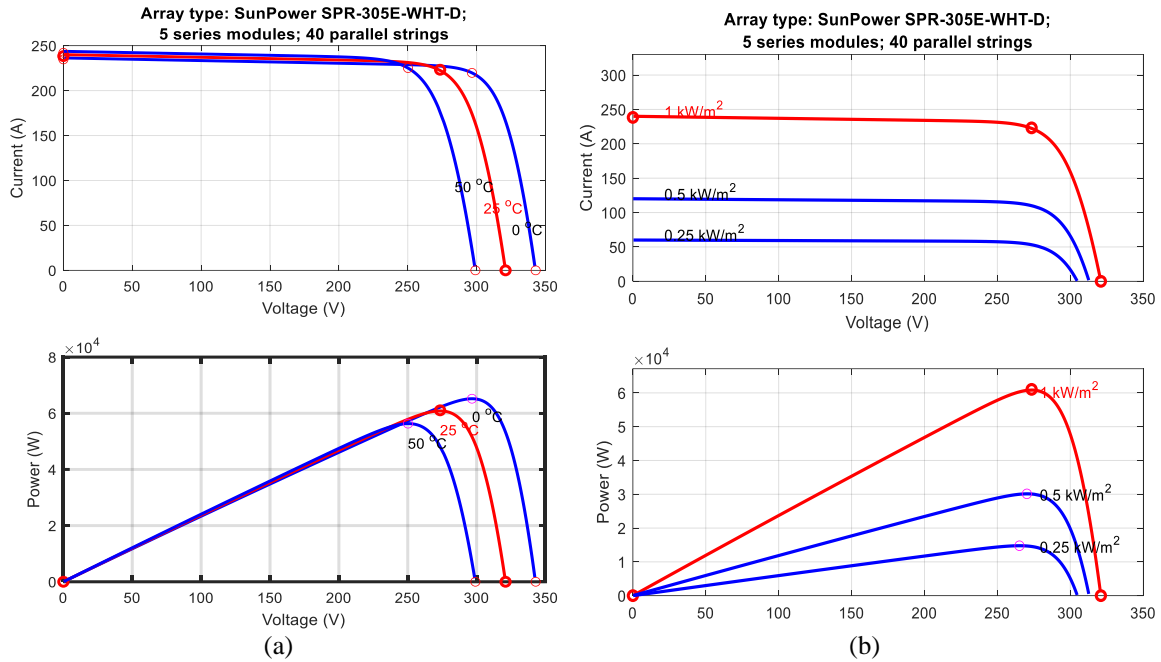


Figure 3. PV current and power versus voltage characteristic (a) for different levels of temperature and (b) for various solar irradiation levels

2.2.1. Perturb and observe (P&O) method

The P&O approach adjusts the output terminal voltage of the PV on a regular basis to compare the power generated during the current cycle to the power generated during the previous cycle. The operating point is changed by the control system either in the direction of the voltage variation and power increase or in the other way. The current is modified slowly after the direction of the change in the current is recognized. In order to achieve a balance between quicker reaction and fewer fluctuations in steady state, this rate is a parameter that should be changed. Figure 4 shows the flowchart for this method. A P&O method is created when the steps are adjusted in accordance with the MPP's distance, leading to greater efficiency. Despite the MPP, each MPPT cycle causes a disturbance in the PV's output terminal voltage. is obtained, which is a common issue P&O technique and results in a loss of power.

2.2.2. Incremental conductance IC method

The widely used incremental conductance based MPPT control inc-con is based on the measurement of solar panel voltage and current for a specific frequency and is used in conjunction with solar panels. As shown in Figure 3(b), the measurement findings indicate that the power slope of the PV is null at MPP (dP/dV = 0), positive to the left and negative to the right. This circumstance makes it possible to calculate the MPP in terms of the increase in array conductance. With the aid of (1), the IC circumstances recommended by (2).

$$\frac{dp}{dv} = \frac{d(v.i)}{dv} = i + v \frac{di}{dv} = 0 \tag{1}$$

$$\frac{\Delta i}{\Delta v} = -\frac{i}{v} \dots \dots (a), \frac{\Delta i}{\Delta v} > \frac{i}{v} \dots \dots (b), \frac{\Delta i}{\Delta v} < \frac{i}{v} \dots \dots (c) \tag{2}$$

Where (2.a) represents the situation at the MPP, (2.b) represents the situation to the left, and (2.c) denotes the situation to the right of the MPP. This method, like P&O, seeks the MPP and has a modified version; however,

it is not essential to calculate the PV output power, and it exhibits excellent transient performance when subjected to fast changes in air conditions. Figure 5 illustrates the IC method's flowchart.

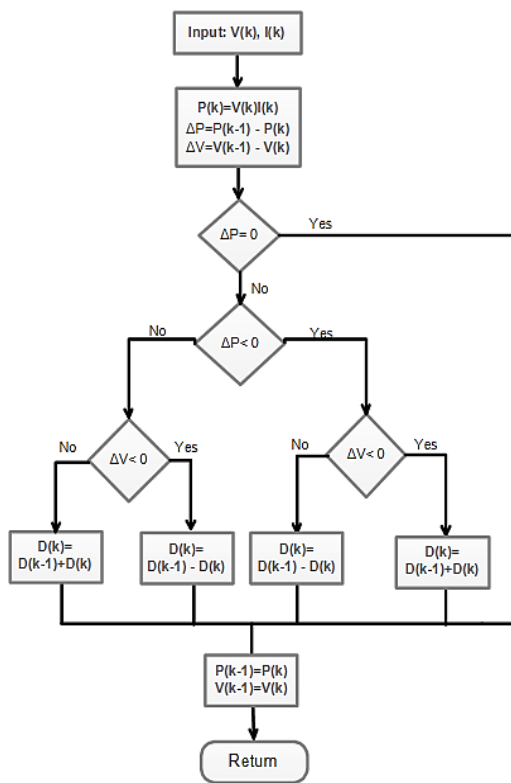


Figure 4. Flowchart of the P&O algorithm

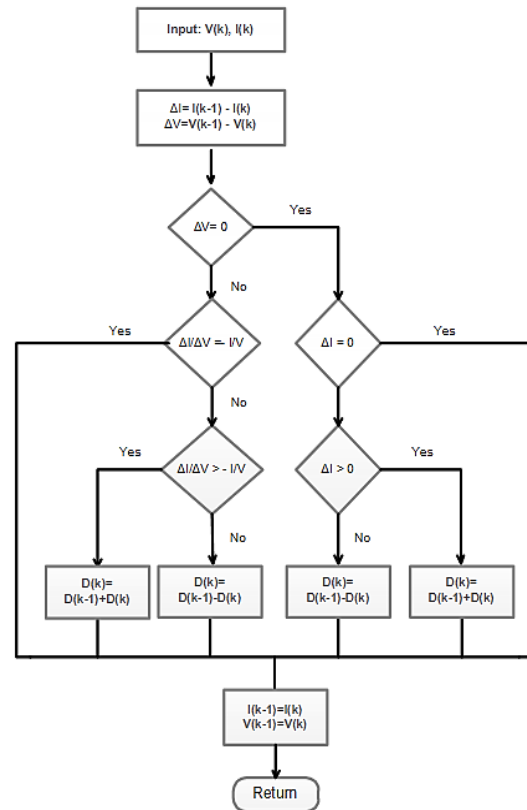


Figure 5. Flowchart of the IC algorithm

2.3. DC-DC boost converter soft switching

The boost converter is also utilized as a DC-DC electrical power interface between the battery load and the solar panel to provide the best matching. The solar module's output voltage is used as the input parameter, and it is adjusted to the required level while maintaining a constant output voltage. A boost chopper's output voltage is always higher than or equal to its input voltage. It utilizes the same parts as the buck converter for easier comparison. The steady-state and dynamic studies of ideal and non-ideal circuits are part of the boost converter investigation. Happening when the ZVS circuit is being created, the auxiliary device must also be able to switch under the ZCS- ZVS condition on its own. The proposed PWM zero voltage transition (ZVT) boost converter is depicted in Figure 1. The sub-circuit is made up of the auxiliary devices S1, C1, D3, Lr, and D4 create desirable switching conditions for the main device S2. To offer ZVS switching, Lr and C1 combine to form the resonant tank. The charge across S2 is to be removed via the path that D3 and Lr produced in order to provide the ZVS condition. The parallel addition of C2 and the primary switch S2 are made to provide ZVS during turn-off. The seven topological stages that the proposed boost converter travels through during one switching cycle are seen in Figures 6 and 7, along with the essential waveforms for each stage. Several assumptions are established throughout each switching cycle in order to streamline the probing of operation modes [10]-[11].

- All the circuit components considered to be ideal.
- The input filter inductor L1 is sufficiently big to permit the use of the filters as a continuous current sink, Iin.
- Because the output capacitors C01 and C02 are sufficiently enough, their voltages are set at Vo.
- The input capacitor Cin is sufficiently large and has set voltages of Vi.

The purpose of the research is to establish a simple design-oriented formula, therefore the on-resistances of the transistors, the DC resistance of the inductor, and the forward voltage drops of the diodes are not taken into account. Figure 6 shows how the active switches are operating. Figure 2 illustrates the key waveforms of the converter's theoretical steady state. As a result, each cycle of the converter has seven switching stages as illustrated in Figures 7 (a) to 7(g). Before starting a new cycle, the auxiliary switch S1 was switched on and the main switch S2 was turned off. The output current was being carried by the rectifier diode D0, while the constant inductor current (Iin) was flowing via D3.

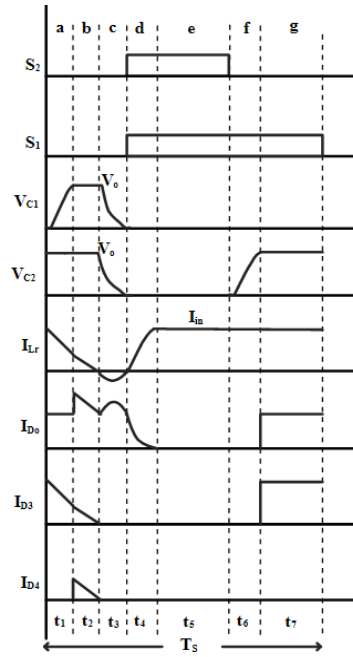


Figure 6. Significant waveforms of the proposed converter

– Stage a: C₁–Capacitor charging mode (t₀-t₁)

When S₁ is turned off by the clock signal, a new cycle begins. As it approaches V_o, the voltage across S₁, V_{C1} parasitic capacitance increases (before being clamped by D₄). D_o keeps transporting the input current. Finding the converter waveform expressions requires solving the linear circuit of Figure 7(a).

$$\begin{aligned} V_{C1}(t) &= Z_1 I_{in} \sin(\omega_1 t) \\ i_{Lr}(t) &= I_{in} \cos(\omega_1 t) \\ V_{C2}(t) &= V_o \end{aligned} \tag{3}$$

Where:

$$Z_1 = \sqrt{\frac{L_r}{C}}, \text{ and } \omega_1 = \frac{1}{\sqrt{L_r C}} \tag{4}$$

C = C₁ = C₂. S₁ and S₂ were considered to be identical switches. The starting conditions are as follows:

$$V_{C1}(0) = 0, \quad V_{C2}(0) = V_o, \quad i_{Lr}(0) = I_{in}$$

and the final condition is

$$V_{C1}(t) = V_{C2}(t) = V_o, \quad i_{Lr}(t_1) = I_{in} \sqrt{1 - \alpha^2}$$

with

$$\alpha = \frac{V_o}{Z_1 I_{in}}$$

providing the period of the first stage

$$t_1 = \frac{\sin^{-1} \alpha}{\omega_1} \tag{5}$$

V_{D4} = 0 when V_{C1} reaches V_o, and D₄ is turned on with ZVS when V_{C1} reaches V_o. The commutation process exhibits zero capacitive turn-on loss.

– Stage b: Resonant inductor discharging mode (t_1 - t_2)

Until the inductor current i_{Lr} reaches zero, L_r is discharged via the path D_0 - V_0 - D_3 - L_r - D_4 . The entire current ($I_{in}+I_{D3}$) is still carried by D_0 . This step is crucial to the converter's design because it discharges the inductor before the multi resonance stage, preventing a peak in the inductor current caused by resonance. The waveform expressions are discovered to be as.

$$\begin{aligned} V_{c1}(t) &= V_0 \\ V_{c2}(t) &= V_0 \\ i_{Lr}(t) &= I_{in}\sqrt{1-\alpha^2} - \frac{V_0}{L_r}t \\ V_{c1}(t_2) &= 0, V_{c2}(t_2) = 0, i_{Lr}(t_2) = 0 \end{aligned} \quad (6)$$

When the stage is complete. The duration of the stage is

$$t_2 = \frac{L_r I_{in}}{V_0} \sqrt{1-\alpha^2} \quad (7)$$

D_3 and D_4 are automatically switched off when I fall to zero.

– Stage c: three-element resonance mode(t_2 - t_3)

In this period, the resonance of L_r , C_1 , and C_2 causes simultaneous zeroing of V_{C1} , V_{C2} , and I_{Lr} . This circumstance causes S_1 and S_2 to turn on at zero voltage and zero current. Because the switches are only active when the current and voltage are zero, they do not incur any capacitive turn-on loss, unlike other converters discussed in the literature. Below are the current and voltage expressions.

$$\begin{aligned} V_{c1}(t) &= V_{c2}(t) = \frac{V_0}{2}(1 + \cos \omega_e t) \\ i_{Lr}(t) &= -\frac{V_0}{Z_e} \sin \omega_e t \\ i_{D_0}(t) &= I_{in} - i_{Lr}(t) \end{aligned} \quad (8)$$

Were

$$C = C_1 = C_2, Z_e = \sqrt{\frac{2L_r}{C}}, \text{ and } \omega_e = \frac{1}{\sqrt{L_r C/2}} \quad (9)$$

The duration's termination is decided by:

$$\begin{aligned} V_{c1}(t_3) &= 0, V_{c2}(t_3) = 0, i_{Lr}(t_3) = 0 \\ t_3 &= \frac{\pi}{\omega_e} \end{aligned} \quad (10)$$

the largest absolute value of I_{Lr} at this point is:

$$i_{Lr} \max = \frac{V_0}{Z_e} \quad (11)$$

while C is an equivalent parasitic capacitance of μF , order, $L \gg C$, indicates that is a low value of (11). During this stage, the current flowing through D_0 is:

$$i_{D_0} = I_{in} + \frac{V_0}{Z_e} \sin(\omega_e t) \quad (12)$$

with

$$i_{D_0} \max = I_{in} + \frac{V_0}{Z_e} \quad (13)$$

In the proposed circuit, this is the lone instance of an overstressed switch. However, because (11) is so insignificant, this stress does not call for an increase in D_0 .

– Stage d: resonant inductor charging mode (t_3 - t_4)

The ZVS is used to turn on S_1 and S_2 to start the stage. Zero turn-on losses for the capacitor are a characterize of the commutation. Up till it reaches, the inductor current increases linearly (I_{in}). This period is when

$$V_{c1}(t_3) = 0, V_{c2}(t_3) = 0, i_{Lr}(t_3) = \frac{V_o}{L_r} t$$

with the final conditions

$$V_{c1}(t_4) = 0, V_{c2}(t_4) = 0, i_{Lr}(t_4) = I_{in}$$

showing the duration of the period as

$$t_4 = \frac{I_{in} L_r}{V_o} \quad (14)$$

as $i_{D_o}(t) = I_{in} - i_{Lr}(t)$

i_{D_o} equals 0 at the conclusion of the interval, and D_o automatically turns off.

– Stage e: Controlled mode (t_4 - t_5)

During this stage

$$V_{c1}(t_4) = 0, V_{c2}(t_4) = 0, i_{Lr}(t_4) = I_{in} \quad (15)$$

The input is kept separate from the output during this time, and a steady current flow from the input filter inductor to the resonant inductor L_r . The feedback loop that controls the output voltage controls how long this stage lasts.

$$D = \frac{t_5}{T_s} \quad (16)$$

Where: T_s is Switching period.

– Stage f: Capacitor C_2 charging mode (t_5 - t_6):

At ZVS, S_2 is opened to start Stage 6 operation, which will charge C_2 with a continuous current. The present stage is concluded when $V_{c2} = V_o$, at which point diodes D_3 and D_o conduct.

$$\begin{aligned} V_{c1}(t) &= \frac{I_{in}}{C_2} t \\ i_{Lr}(t) &= I_{in} \\ i_{D_o}(t) &= 0 \\ V_{D_o}(t) &= V_o - V_{c2} \end{aligned} \quad (17)$$

At the end this stage, allowing for D_o to turn on with ZVS, and $V_{c2}(t_6) = V_o$ and the duration is:

$$t_6 = \frac{V_o C_2}{I_{in}} \quad (18)$$

– Stage g: freewheeling mode (t_6 - t_7)

While the current in L_r freely oscillates between D_3 and S_1 , the energy stored in the filter inductor is released into the output capacitor and load at this point. The duration's conclusion is dictated by (19).

$$V_{c1}(t_7) = 0, V_{c2}(t_7) = 0, i_{Lr}(t_7) = I_{in}, i_{D_o}(t_7) = I_{in} \quad (19)$$

The suggested converter accomplishes soft switching without any capacitive turn-on losses by turning off the auxiliary switch S_1 at time t_7 and starting to charge C_1 to voltage V_o at the beginning of the new switching cycle. Conduction loss on the additional switch S_2 is the cost of this accomplishment. However, S_2 is only used for the first two stages, limiting losses.

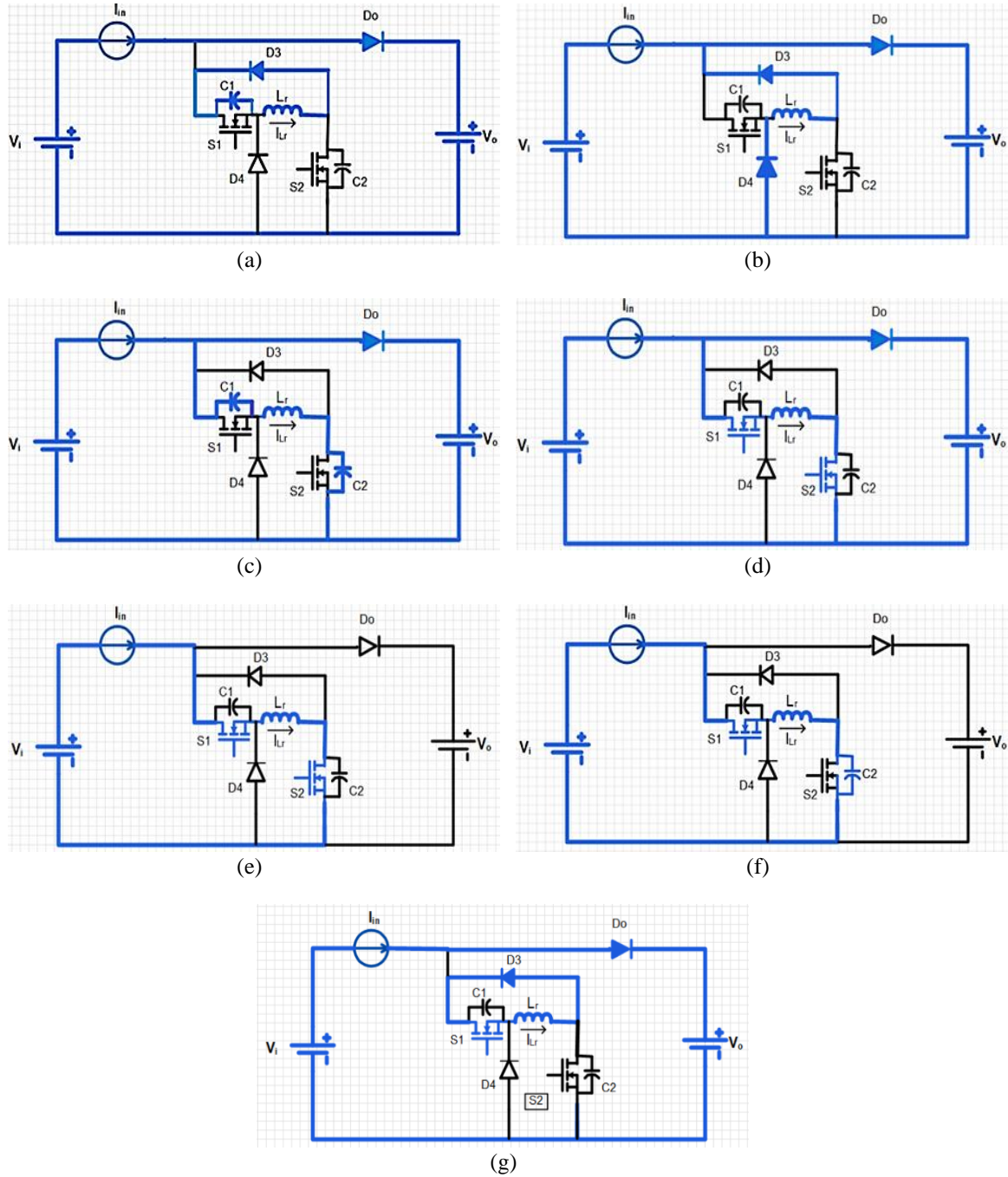


Figure 7. Boost converter topological stages during a switching cycle (a) C_1 -capacitor charging, (b) resonant inductor discharging, (c) three-element resonance, (d) resonant inductor charging, (e) controlled stage, (f) C_2 -capacitor charging and (g) free-wheeling stage

2.4. Conversion ratio (M) and relation with duty ratio (D)

The equation for D in terms of M ($M = V_o/V_i$) is obtained by equating the energy of the converter's input and output. The typical method of considering 100% efficiency [11] is also employed in this case, since the average diode current generates the average output current when the diode is connected to the load side. Both the energy output (W_o) and the energy input (W_i) every cycle is equal.

$$W_i = V_i I_{in} T_s, \quad W_o = V_o \int_0^{T_s} i_{D_o} dt \tag{20}$$

The relationship between the conversion and duty ratio is shown below. This is done by substituting the correct input and diode currents, which can be found by solving for the corresponding stages in the above equation.

$$D = \left(\frac{(M-1)}{M} \right) - \frac{M\alpha^2}{K} \quad (21)$$

Were,

$$K = \frac{2R_L}{L_r f_s} \quad (22)$$

f_s is the switching frequency

The terms in the second bracket can be shown to have tiny values in comparison to the term $(M-1)/M$ for practical values; as a result, the new converter's duty ratio is quite similar to the boost converter's conventional duty ratio. The previous equation also demonstrates how well the converter controls the load and how changes in the load have very little influence on D .

2.5. Condition for ZVS

At the end of stage "c", the capacitor voltages V_{C1} and V_{C2} must be drained to zero in order to establish the necessary conditions for ZVS. If V_{C1} is equal to V_o at the end of stage "a" then this is possible. It may be shown that both of the above criteria can be satisfied if:

$$\alpha < 1 \quad (23)$$

in (23) gives the design formula for L_r :

$$L_r > \frac{V_{omax}^2}{I_{in min}^2} C \quad (24)$$

this gives the design value for L_r .

3. RESULTS OF SIMULATION FOR PV ARRAY WITH MPPT CONTROLLER AND DC SOFT SWITCHING BOOST CONVERTER

On the basis of the block diagram in Figure 2, an expanded model of a PV array with a DC soft switching boost converter and an MPPT controller was developed. In Figure 8, the model controller is displayed. The solar irradiance and temperature of the PV array are again used as inputs for the extended model, which are used to determine the PV array's output current, voltage, power, and open circuit voltage. The MPPT controller model uses the computed PV array voltage and open circuit voltage to adjust the boost converter duty cycle D using the two techniques shown in the flowcharts in Figures 4 and 5. For the DC soft switching boost converter to operate, the main and auxiliary switches are triggered in accordance with the theoretical description shown in Figure 6. The specifications for the PV array are shown in Table 1, while the parameters of the DC soft switching boost converter are shown in Table 2.

Figures 9 and 10 display the simulation results for the soft switching boost converter with MPPT controller (a and b). The MATLAB simulation, in which V_{C1} , V_{C2} , and I_{Lr} reach zero before S_1 and S_2 are turned on, shows the zero-voltage and ZCS of S_1 and S_2 . The input and output voltages of the soft-switching boost converter at varying levels of solar irradiation and temperatures are shown in Figure 11 using various MPPT controllers for the PV array.

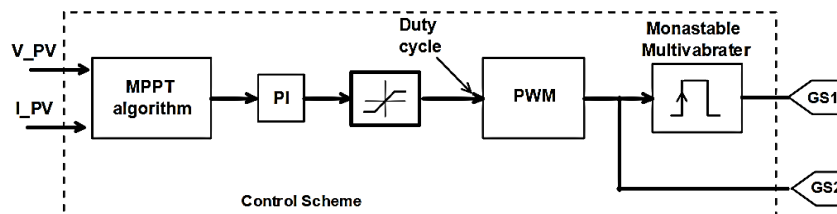


Figure 8. The model controller for generating pulses to drive gates, main and auxiliary switches

Table 1. Technical parameters of use PV panels

Parameter name	Parameter value
Open circuit voltage	64.2V
Max. power	305.226 W
Voltage at the point of maximum power V_{mp}	54.7 V
Temperature coefficient of $V_{oc}(\%/deg.C)$	-0.27269
Bandgap voltage for silicon	1.11 [eV]
Short-circuit current	5.96[A]
Current at maximum power point ISC	5.58 A
Temperature coefficient of Isc ($\%/deg.C$)	0.061745
Serial resistance	0.37152 [Ω]
Parallel resistance	269.5934 [Ω]

Module: SunPower SPR-305E-WHT-D

Table 2. Circuit parameters of DC soft switching converter

Components	Value	Unit
Input voltage, V_{in}	300	V
Output voltage, V_o	500	V
Resonant inductor, L_r	150	μH
Resonant capacitor, C_1	1	μf
Resonant capacitor, C_2	1	μf
Output Capacitor C_{o1}	12	mf
Output Capacitor C_{o2}	12	mf
input Capacitor C_{in}	100	μf
input inductor, L_{f1}	5	mH
Output power	60	kW
Switching frequency	5	kHz
Minimum duty cycle	0.4	-
Maximum duty cycle	0.6	-

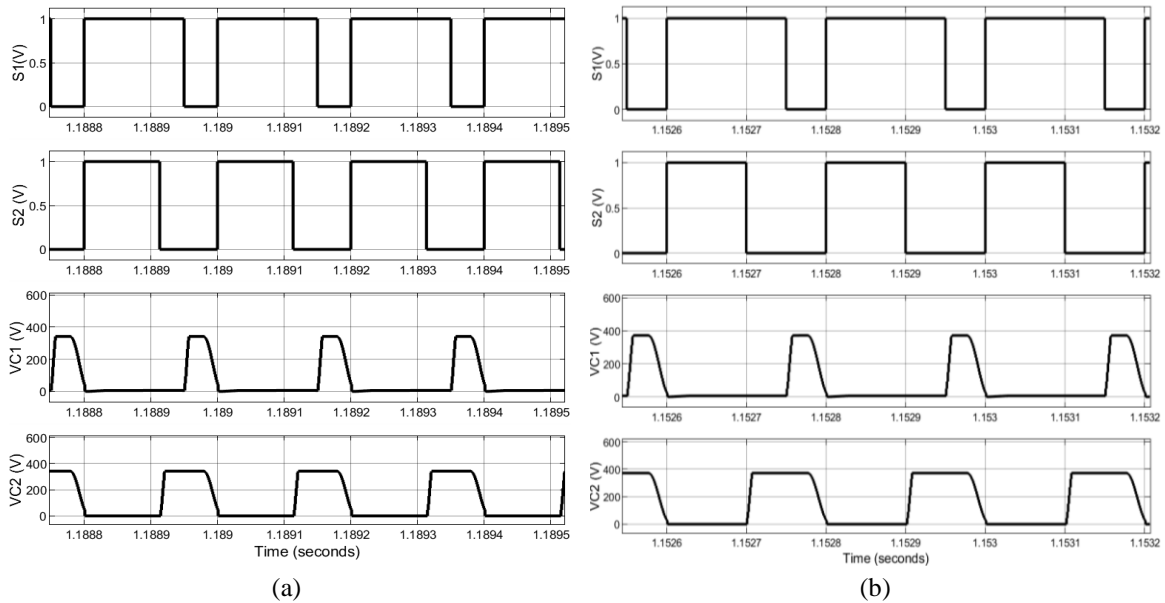


Figure 9. Soft switch boost converter with MPPT controller simulation results; (1) gate signal S1 (2) gate signal S2 (3) voltage capacitor C1 (4) voltage capacitor C2, (a) P&O method and (b) IC method

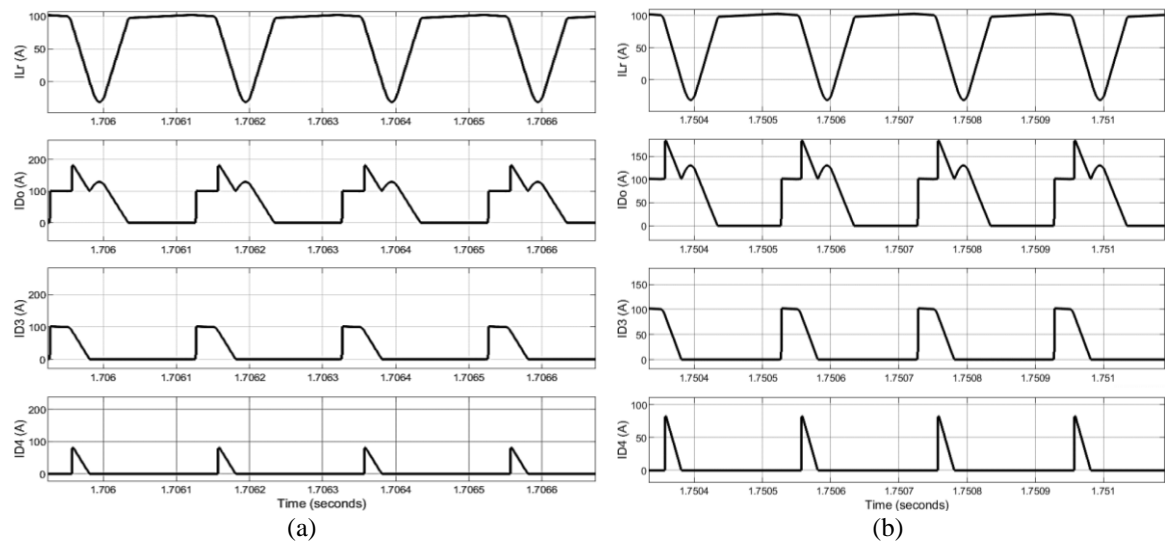


Figure 10. Soft switch boost converter with MPPT controller simulation results; (1) current inductor L_r (2) current I_{D_o} (3) current I_{D_3} and (4) current I_{D_2} , (a) P&O method and (b) IC method

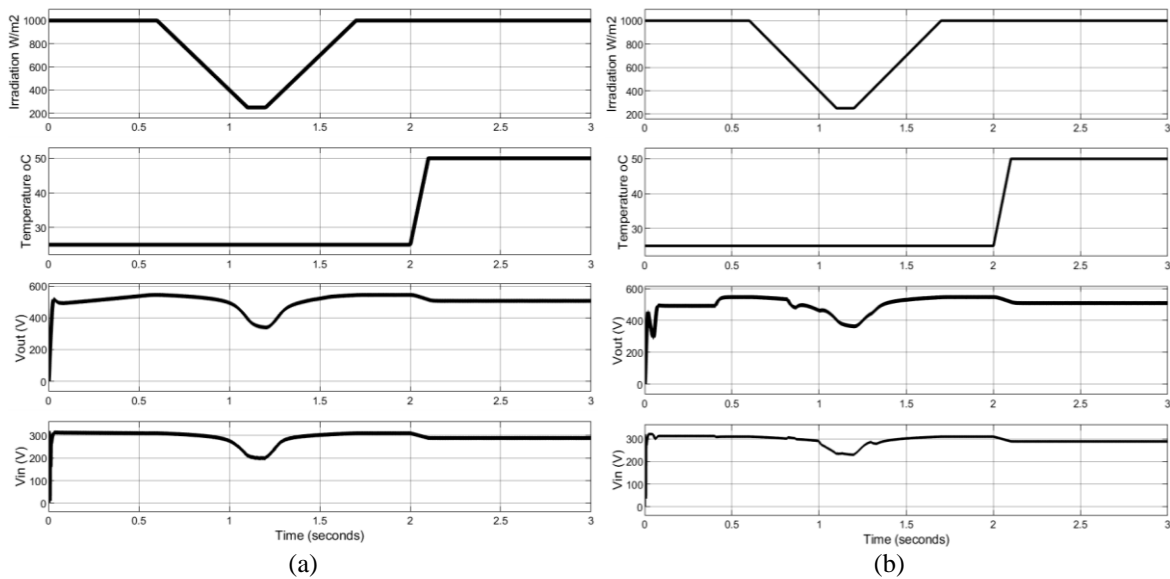


Figure 11. Simulation results of the photovoltaic characteristics; 1) solar irradiation, 2) temperature, 3) voltage output soft switching boost converter, and 4) voltage output PV array and input to the soft switching boost converter: (a) P&O method and (b) IC method

Using different MPPT controllers, Figure 12 shows the PV array's power, current, voltage, and duty cycle curves for changed solar irradiation and temperature. To simulate the load variation controlled by MATLAB/Simulink, the DC-DC boost converter's soft switching model was utilized. It also included a fluctuation to imitate the impact of the inductor ripple current. As shown in Figure 11, all experiments were conducted while taking the same temperature and irradiance changes into consideration. The responses of the top MPPT algorithms were analyzed, and the graph of PV power extracted highlights the maximum possible power. It becomes vital to offer performance measurements that may be utilized as comparison criteria in order to compare and tweak each algorithm suitably according to the application. There are extra metrics that are used in these situations in addition to the standard metrics for dynamic responses. Regarding their dynamic reaction, or how they act when the power panel is minimal and quickly adjusted to the nominal situation, MPPT approaches should be contrasted. For the sake of testing, the output power ranges instantly from 11.7 KW to 30.6 KW and may be assessed using Figure 12. According to the results, P&O procedures and IC approaches seem to require less time to reach a steady state (time of the order of 0.2 s). Just to emphasise the techniques, P&O and IC employed the same approach to search for MPPT, which is dP/dV null at MPP, and as a result, their quality indices were quite similar. A DC soft switching boost converter can function in seven different modes, in accordance with the theoretical description that was previously provided. The switching impulses produced by the MPPT controller are what cause a state to transition from one to the next. The MATLAB/Simulink model is ideal in these situations because it makes it simple to combine several representations of the model's object dynamic operation by simply specifying the right amount of states and transitions between them. As a consequence, MATLAB/Simulink was used to create the model of the DC soft-switching boost converter [8]. The results from the extended model were consistent with theoretical predictions and were comparable to those from the simple PV array model using a DC hard switching boost converter. However, the expanded model also shows the beneficial effects of a DC soft switching boost converter with an MPPT controller, resulting in generating power that is nearly higher than that of the simple model. This converter has the advantage of increasing circuit power efficiency and reducing switch power loss.

As demonstrated in Figures 13(a) and 13(b), the solar photovoltaic (PV) power systems with proposed converter achieves an overall efficiency of 98% for various levels of solar irradiation (100 to 1000 W/m²) and temperature (25 to 50 °C), with a maximum output power of 30.6 KW and a switching frequency of 5 kHz. Even at low output powers, the efficiency is virtually equivalent to that of a comparable converter described in [10], and it can be demonstrated that the efficiency levels are higher than those of most other Soft Switching (SS) converters. Because the new converter is particularly sensitive to recirculated energy, as the load current reduces, so does the converter loss. Finally, the simulation results validated the theoretic analysis of the proposed ZVT-boost converter.

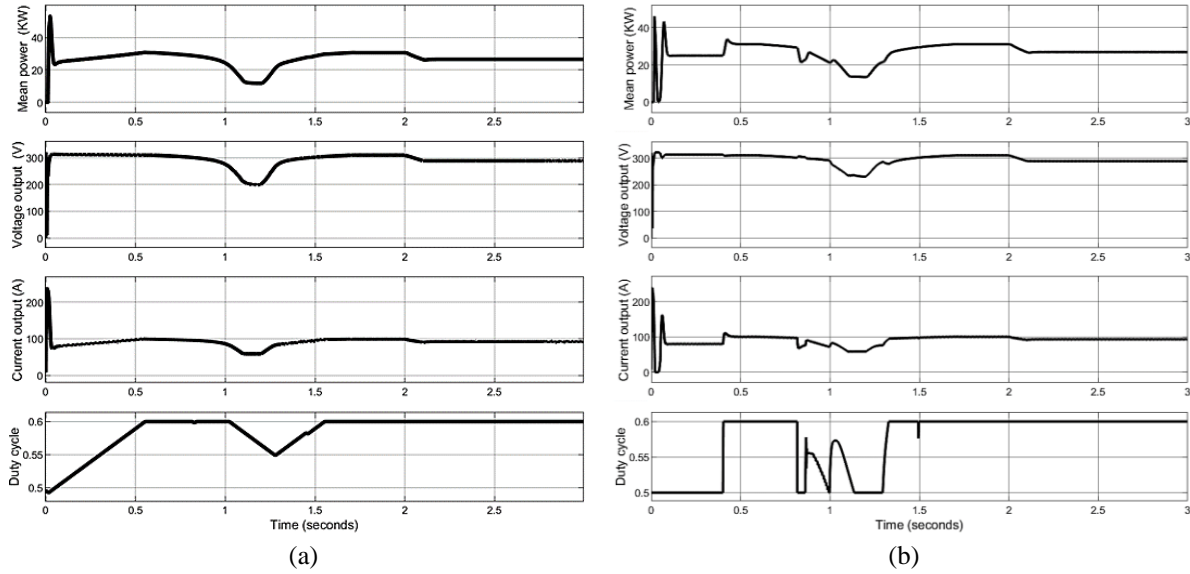


Figure 12. Simulation results of the photovoltaic characteristics; 1) mean power to PV array, 2) Voltage output PV array, 3) current output PV array, and 4) duty cycle: (a) P&O method and (b) IC method

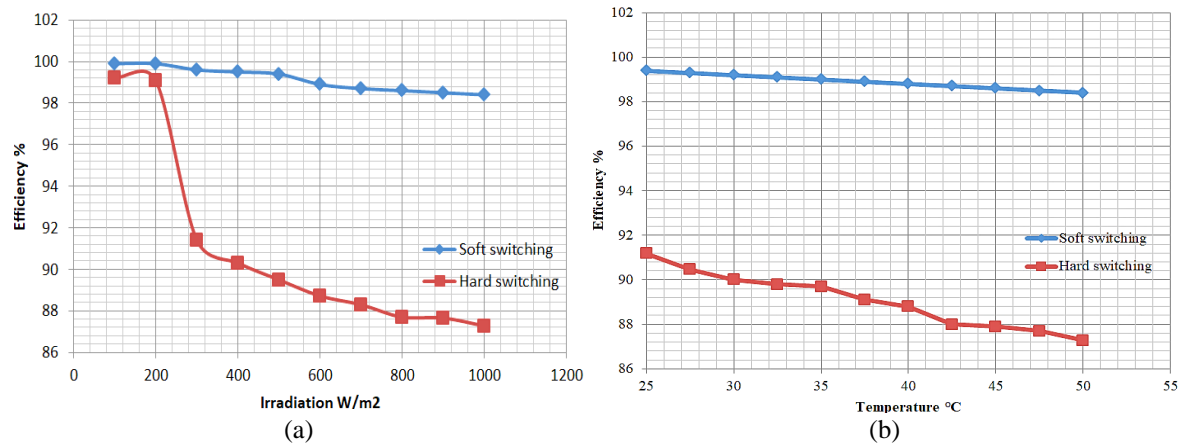


Figure 13. Comparing soft switching (SS) and hard switching (HS) boost converter efficiency curves, (a) for different levels of solar irradiation and (b) for different levels of temperature

4. CONCLUSION

Solar energy is very important in modern times. Because it is a resource for energy production that is freely accessible. However, the solar system's efficiency is the sole issue. Additionally, to improve efficiency, the soft switching boost converter is controlled by maximum power point approaches (MPPT) techniques. The active switches in the converter experience zero capacitive turn-on losses, in contrast to switches in other soft-switched topologies discussed in the literature. The converter is subjected to a thorough mathematical examination in steady-state conditions. The simulation results demonstrate that the algorithm in this research can implement grid-connected power generation of the grid-connected soft switching boost converter and high reliability and cheap cost.




The MPP changes as a result of changes in cell temperature or irradiance on the PV module characteristic curve. To maximize the effectiveness of the PV system, continual tracking to the MPP is therefore necessary. To accomplish the latter, a DC-DC soft switching boost converter is positioned between a PV module and a load, and an MPPT algorithm is used to establish the proper duty ratio (D), which controls the switching of the converter. A successful MPPT technique strikes a balance between tracks speed and steady-state accuracy and demonstrates a quick reaction during unexpected environmental changes. These criteria show that the proposed soft switching boost converter can be used with both IC and P&O approaches because they have similar quality indices. Future research will concentrate on an ultra-high gain DC-DC converter with

a single-switch design that can be utilized in fuel cell and photovoltaic systems because of its structural and functional characteristics, including low input current ripple, high voltage gain, acceptable efficiency, and soft switching performance.




REFERENCES

- [1] S. Sumathi, L. Ashok Kumar, and P. Surekha, "Solar PV and wind energy conversion systems: introduction to theory, modeling with MATLAB/SIMULINK, and the role of soft computing techniques," *Green Energy and Technology*, p. 807, 2015, [Online]. Available: <http://link.springer.com/10.1007/978-3-319-14941-7>.
- [2] N. Ramalingam *et al.*, "Implementation of PI controller for boost converter in PV system," *International Journal of Advanced Research in Management, Architecture, Technology and Engineering (IJARMATE)*, vol. II, no. April, pp. 6–10, 2016.
- [3] N. E. Zakzouk, M. A. Elshaharty, A. K. Abdelsalam, A. A. Helal, and B. W. Williams, "Improved performance low-cost incremental conductance PV MPPT technique," *IET Renewable Power Generation*, vol. 10, no. 4, pp. 561–574, 2016, doi: 10.1049/iet-rpg.2015.0203.
- [4] M. A. Omar and M. M. Mahmoud, "Improvement approach for matching pv-array and inverter of grid connected pv systems verified by a case study," *International Journal of Renewable Energy Development*, vol. 10, no. 4, pp. 687–697, 2021, doi: 10.14710/ijred.2021.36082.
- [5] M. Latkova, M. Bahernik, P. Bracinik, and M. Hoger, "Modelling of a dynamic cooperation between a PV array and DC boost converter," *IYCE 2015 - Proceedings: 2015 5th International Youth Conference on Energy*, 2015, doi: 10.1109/IYCE.2015.7180783.
- [6] Z. Fang, Y. Yang, Z. Lu, A. Yang, and X. He, "Circuit simulation of MPPT charge regulator based on soft switching," *2022 5th International Conference on Energy, Electrical and Power Engineering, CEEPE 2022*, pp. 210–215, 2022, doi: 10.1109/CEEPE5110.2022.9783395.
- [7] S. H. Park, G. R. Cha, Y. C. Jung, and C. Y. Won, "Design and application for PV generation system using a soft-switching boost converter with SARC," *IEEE Transactions on Industrial Electronics*, vol. 57, no. 2, pp. 515–522, 2010, doi: 10.1109/TIE.2009.2036025.
- [8] M. Y. Worku and M. A. Abido, "Grid connected PV system using ANFIS based MPPT controller in real time," *Renewable Energy and Power Quality Journal*, vol. 1, no. 14, pp. 35–40, 2016, doi: 10.24084/repqj14.220.
- [9] S. R. Pendem and S. Mikkili, "Modeling, simulation and performance analysis of solar PV array configurations (Series, Series-Parallel and Honey-Comb) to extract maximum power under Partial Shading Conditions," *Energy Reports*, vol. 4, pp. 274–287, 2018, doi: 10.1016/j.egy.2018.03.003.
- [10] B. P. Divakar and A. Ioinovici, "PWM converter with low stresses and zero capacitive turn-on losses," *IEEE Transactions on Aerospace and Electronic Systems*, vol. 33, no. 3, pp. 913–920, 1997, doi: 10.1109/7.599311.
- [11] B. P. Divakar, K. W. E. Cheng, and D. Sutanto, "Zero-voltage and zero-current switching buck-boost converter with low voltage and current stresses," *IET Power Electronics*, vol. 1, no. 3, pp. 297–304, 2008, doi: 10.1049/iet-pel:20070038.
- [12] Y. Yao, Y. Fang, H. Xiong, Z. Tian, S. Cao, and Y. Xie, "Study on quasi resonant grid-connected current compensation method with controllable switching period," *Proceedings of the IEEE International Conference on Industrial Technology*, pp. 225–229, 2017, doi: 10.1109/ICIT.2017.7913087.
- [13] A. S. Lalitha, S. Chakraborty, and S. S. Kumar, "A zero voltage switching based soft switching boost DC-DC converter for vehicle to grid applications with enhanced energy efficiency," *2022 3rd International Conference for Emerging Technology, INCET 2022*, 2022, doi: 10.1109/INCET54531.2022.9824207.
- [14] N. Femia, G. Petrone, G. Spagnuolo, and M. Vitelli, "Optimizing duty-cycle perturbation of P&O MPPT technique," *PESC Record - IEEE Annual Power Electronics Specialists Conference*, vol. 3, pp. 1939–1944, 2004, doi: 10.1109/PESC.2004.1355414.
- [15] T. Esmar and P. L. Chapman, "Comparison of photovoltaic array maximum power point tracking techniques," *IEEE Transactions on Energy Conversion*, vol. 22, no. 2, pp. 439–449, 2007, doi: 10.1109/TEC.2006.874230.
- [16] H. Kaushik and B. Bhushan, "Performance analysis of boost converters in a PV system with P and O based MPPT controller connected to a battery backup and grid," *2022 IEEE Delhi Section Conference, DELCON 2022*, 2022, doi: 10.1109/DELCON54057.2022.9752878.
- [17] M. Gupta and R. Gupta, "Performance evaluation of boost DC-DC converter for different loads to extract maximum power from solar PV module," *2022 IEEE Delhi Section Conference, DELCON 2022*, 2022, doi: 10.1109/DELCON54057.2022.9753493.
- [18] D. Rastogi, M. Jain, and M. Sreejeth, "Comparative study of DC-DC converters in PV systems using fuzzy logic MPPT algorithm," *2022 IEEE Delhi Section Conference, DELCON 2022*, 2022, doi: 10.1109/DELCON54057.2022.9753494.
- [19] R. Divya, A. R. Nair, S. Harisankar, V. G. S. Sai, and M. G. Nair, "Illustration of maximum power point tracking of photovoltaic array with boost converter via perturb and observe algorithm," *2022 4th Asia Energy and Electrical Engineering Symposium, AEEES 2022*, pp. 992–996, 2022, doi: 10.1109/AEEES54426.2022.9759789.
- [20] S. R. Pendem and S. Mikkili, "Performance evaluation of series, series-parallel and honey-comb PV array configurations under partial shading conditions," *2017 7th International Conference on Power Systems, ICPS 2017*, pp. 749–754, 2018, doi: 10.1109/ICPES.2017.8387389.
- [21] Z. Mehmood, Y. Bilal, M. Bashir, and A. Asghar, "Performance analysis of MPPT charge controller with single and series/parallel connected PV panels," *2016 International Conference on Intelligent Systems Engineering, ICISE 2016*, pp. 278–282, 2016, doi: 10.1109/INTELSE.2016.7475134.
- [22] A. M. Othman, M. M. M. El-arini, A. Ghitas, and A. Fathy, "Realworld maximum power point tracking simulation of PV system based on Fuzzy Logic control," *NRIAG Journal of Astronomy and Geophysics*, vol. 1, no. 2, pp. 186–194, 2012, doi: 10.1016/j.nrjag.2012.12.016.
- [23] A. Chitransh and M. S. Kumar, "The different type of MPPT techniques for photovoltaic system," *Indian Journal of Environment Engineering*, vol. 1, no. 2, pp. 1–4, 2021, doi: 10.54105/ijee.a1809.111221.
- [24] S. Abbasian, H. S. Gohari, M. Farsijani, K. Abbaszadeh, H. Hafezi, and S. Filizadeh, "Single-switch resonant soft-switching ultra-high gain DC-DC converter with continuous input current," *IEEE Access*, vol. 10, pp. 33482–33491, 2022, doi: 10.1109/ACCESS.2022.3161456.
- [25] A. Haddou, N.-E. Tariba, N. Ikken, A. Bouknadel, H. El Omari, and H. El Omari, "Comparative study of new MPPT control approaches for a photovoltaic system," *International Journal of Power Electronics and Drive Systems*, vol. 11, no. 1, p. 251, 2020, doi: 10.11591/ijpeds.v11.i1.pp251-261.




BIOGRAPHIES OF AUTHORS

Basim Talib Kadhem    received his B.Sc degree in electrical engineering from the Engineering College at the University of Basrah in 1998. He received his Master's degree from the same university in 2001. In 2009, He got his PhD from the College of Engineering, Department Electrical Engineering of Electrical Power Systems and Networks, St-Petersburg State Polytechnical University, Russia. He is now a faculty member at the engineering college at the University of Basrah, Iraq. His research interests include soft-switching converters., FACTS and applications of high-power inverters, power circuit modeling, and study, torsional dynamics of powerful steam turbo generators, power system control. He can be contacted at email: basim.kadhem@uobasrah.edu.iq.






Sumer Sahib Hardan    is a Lecturer at the Department of Electrical Engineering at the University of Basrah, Iraq, where he has been a faculty member since 2002. Sumer graduated from the Engineering College/Electrical Engineering Department in 1999 from the University of Basrah and got his Msc in 2006 from the same university. His research interests are primarily in the areas of power electronics, and wireless power transfer. He can be contacted at email: sumer.hardan@uobasrah.edu.iq.



Osama Yaseen Khudair Al-Atbee    is a Lecturer at the Department of Electrical Engineering at the University of Basrah, Iraq, where he has been a faculty member since 2006. Osama graduated from the Engineering College/Electrical Engineering Department in 2001 from the University of Basrah and got his Msc in 2005 from the same university. In 2018, he got his PhD in Electrical Engineering from the Engineering College, University of Leicester, United Kingdom (UK). His research interests are primarily in the areas of renewable energy, power electronics, and micro-grids. He can be contacted at email usama.khader@uobasrah.edu.iq.



Khalid Mahdi Abdhassan    received his B.Sc degree in electrical engineering from the Engineering College at the University of Basrah in 1997. He received his Master's degree from the same university in 2001. In 2011, He got his PhD from the Engineering College/Electrical Engineering Department/University of Basrah, Iraq. He is now a faculty member at the engineering college at the University of Basrah, Iraq. His research interests include control strategies for AC and DC machines and power electronics. He can be contacted at email: Khalid.abdihassan@uobasrah.edu.iq.